C. Xiong, H. Fan, X. Huang, C. Fernandez-Pello (2022) *Evaluation of burning rate in microgravity based on the fuel regression, flame area, and spread rate*, **Combustion and Flame**, 237, 111846. doi: 10.1016/j.combustflame.2021.111846

Evaluation of burning rate in microgravity based on the fuel regression, flame area, and spread rate

Caiyi Xiong[1,2], Haoran Fan[1], Xinyan Huang[1,*], and Carlos Fernandez-Pello[3]

[1]*Research Centre for Fire Safety Engineering, Hong Kong Polytechnic University, Hong Kong SAR*

[2]*The Hong Kong Polytechnic University Shenzhen Research Institute, Shenzhen, China*

[3]*Department of Mechanical Engineering, University of California, Berkeley, CA 94720, USA*

*Corresponding to xy.huang@polyu.edu.hk (X. Huang)

Abstract:

The fuel burning rate and heat-release rate (HRR) play key roles in determining the fire intensity and hazard. On Earth, the burning rate of a condensed fuel is normally measured by the mass loss, but in microgravity, the impossibility of measuring the weight loss with a balance makes the measurement of burning rate challenging. This work proposes three methods to quantify the burning rate of condensed fuels in microgravity by measuring (i) the regression rate of the fuel surface, (ii) the spread rate of the flame leading edge, and (iii) the flame-sheet area, which all rely on video imaging of the flame or fuel surface geometry. The accuracies of these methods are quantified first in the ground-based tests with representative fuels, 1) solid candle and PMMA rods with diameters from 8-15 mm, 2) liquid fuels including propanol, hexane, and kerosene, and 3) the methane and propane gases. Results show that the burning rate obtained optically by tracking the flame leading edge and the fuel regression were less accurate due to strong sensitivity to camera resolution and background light. Comparatively, measuring the flame-sheet area is easier and gives more accurate results, and microgravity PMMA-rod flame (BASS-II project in the International Space Station) show that the fuel mass flux across the flame sheet is almost constant (0.15 mg/cm^2-s) for a given fuel configuration and environment. This work offers a useful way to measure fuel burning rate and HRR in spacecraft and provides a path for the performance-based spacecraft fire safety design.

Keywords: *Microgravity; Condensed fuel; Mass loss rate; Flame-sheet area; Data driven*

Nomenclature

Symbols		v	velocity (mm/s)
A	area (mm^2)	Y	mass fraction (-)
G	weight (g)		
g	gravitational acceleration (m/s^2)	***Greeks***	
ΔH	heat of reaction (kJ/g)	γ	length/pixel ratio (mm/pixel)
HRR	heat release rate (W)	ε	root-mean-square error
L	length (mm)	η	efficiency of combustion
MLR	mass loss rate (mg/s)	ρ	density (g/mm^3)
$\dot{m}''$	mass flux of fuel gas (mg/cm^2-s)		
$\dot{m}$	mass loss rate measured by balance	***Subscripts***	
n	number of sampling data	c	combustion reaction
P	number of pixels	F	fuel
$\dot{R}$	fuel regression rate (mm/s)	f	flame
t	video duration (s)	g	gas fuel
$\dot{V}$	gas flow rate (mm^3/s)	ox	oxidation
V	volume (mm^3)	Ref	reference volume

1. Introduction

On Earth, gravity-induced buoyancy can complicate the flame dynamics [1,2]. Thus, conducting combustion experiments in a microgravity environment makes the flame simpler and helps reveal the fuel-burning and flame characteristics [3–7]. Furthermore, the fire hazard in microgravity is an important concern for space travel, and it will increase as the travel time spent in space is increased with the proposed space missions [8–12]. On the other hand, combustion experiments in a microgravity environment are difficult and expensive to conduct. For this reason, the burnings of small solid fuel samples have been investigated in the limited amount of microgravity combustion experiments, where the flame spread rate and extinction limits are primarily explored [8,13–21].

Although the growing spacecraft experiments continue to yield insights into the microgravity flame and burning characteristics of gaseous fuels, very limited data are available about the burning rate of solid and liquid fuels and the corresponding heat-release rate (HRR). Based on the classical Burke-Schumann's theory [22,23], it is possible to correlate the fuel flow rate and flame shape for a pure diffusion flame. Several studies [24–26] have also combined the theoretical analysis and the flame geometrical information to estimate the fuel burning rate, while these analytical models require accurate input parameters. Considering the experimental approach, the HRR of a burning condensed fuel can be measured by the mass-loss rate [27] or the oxygen depletion of fume gases under the principle of oxygen calorimetry [28]. Nevertheless, a microgravity environment disables the use of regular mass balance to

obtain the mass-loss rate (MLR). Using oxygen calorimetry requires two oxygen sensors mounted in the wind tunnel before and after the flame with a fast response speed [5,29,30], which is also challenging. Moreover, if not all the fuel gases are consumed in the flame, the accuracies of both fuel-based and oxygen-based HRR measurements are reduced. Thus, new indirect methods are needed to quantify the MLR of burning fuels and estimate the HRR in microgravity. The accurate measurement of flame HRR will be valuable for estimating the fire hazards in spacecraft and the performance-based fire safety design of spacecraft facilities.

In most flame-spread and fuel-burning experiments on Earth or in microgravity, video cameras are always used, which record the variation of flame, the spread of flame front, and the regression of fuel sample (e.g., [4,6,7,31]). If the relationships between these parameters measured from videos and the fuel-burning rate can be established, there would be other methods to calculate fuel MLR and fire HRR in microgravity. However, the accuracy and reliability of these methods are still unknown, considering the quality of video footage varies from test to test and can be interfered by experimental and environmental conditions, such as the sizes of flame and fuel, image resolution, and background light.

For this reason, this work aims to explore the feasibility of using the above three parameters, i.e., flame geometry, flame spread, and fuel regression, to measure MLR for different burning fuels. The accuracies of these methods are first examined on the ground with a precision balance for liquid and solid fuels, and a controlled flowmeter for gaseous fuels. The mechanism behind the pros and cons of each method are discussed. Finally, PMMA-rod experiments previously conducted in microgravity (BASS-II project in the International Space Station [14,19]) were used to verify the feasibilities of these three methods in space.

2. Methodology

2.1. Principles of fuel MLR and flame HRR measurements

With gravity, a mass balance can be used to measure the mass-loss rate ($\dot{m}$) of the burning solid and liquid fuels as

$$\dot{m} = \frac{1}{g}\frac{dG}{dt} \tag{1}$$

where G is the weight of fuel sample and g is the gravitational acceleration. If all gasified fuels are completely consumed in the flame, the MLR is also the burning rate [24,25]. For gaseous-fuel flame, the mass flow rate or volume flow rate ($\dot{V}_{F,g}$) is normally controlled and pre-set, Thus, its burning rate under complete combustion is known or proportional to the gas density (ρ_{Fg}) and flow rate ($\dot{V}_{F,g}$) as

$$\dot{m} = \rho_{Fg}\dot{V}_{F,g} \tag{2}$$

For solid and liquid fuels, by choosing a control volume on the condensed fuel surface (see Fig. 1), the mass-loss rate can be indirectly estimated by the volume change of fuel or the regression of fuel surface as

$$MLR = \dot{m}_F = \rho_F \dot{R}_F A_F \qquad \text{[Regression method]} \qquad (3)$$

where ρ_F and A_F are the density and cross-section area of the condensed fuel. Since the changed fuel volume keeps a cylindrical shape, the local regression rate of fuel angle in the vertical direction, $\dot{R}_F$, is used here. This fuel-regression method can be used in microgravity, if the density of the fuel is known, and the evolution of fuel shape can be well captured.

Alternatively, the mass-loss rate can be estimated by the motion of flame leading edge if the flame-spread rate (v_f) is equal to the component of the local regression rate of fuel surface ($\dot{R}_F$) under steady-state burning as

$$\dot{m}_F = \rho_F v_f A_F \qquad \text{[Flame-spread method]} \qquad (4)$$

where the density and cross-section area of the condensed fuels are again needed. Usually, when the environment changes, the flame-spread rate can reach a new steady-state in a few seconds, while it could take a few minutes for the regression rate to reach the new steady-state [32]. Thus, if the process of flame spread is not stable, this flame-spread method is not real-time and has low accuracy.

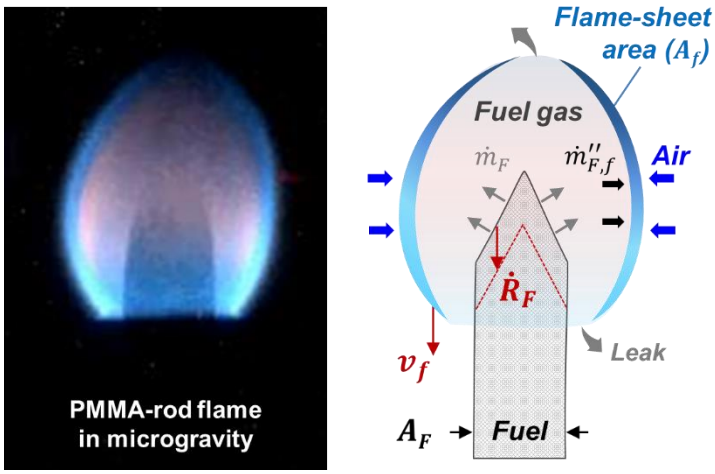

Fig. 1. The PMMA rod flame in microgravity [14] and the illustration of flame spread and fuel burning, where $\dot{m}_F$ is fuel mass-loss (burning) rate, $\dot{m}''_{F,f}$ is the fuel mass flux on the flame sheet, $\dot{R}_F$ is the fuel-regression rate, v_f is the flame-spread rate, A_f is the flame-sheet area, and A_F is the fuel cross-section area.

The mass-loss rate of fuel ($\dot{m}_F$) is also the burning rate of fuel gas ($\dot{m}_{F,g}$). If all the gasified fuels are consumed at the flame, $\dot{m}_F$ can be measured with the control volume of the flame sheet as

$$\dot{m}_F = \dot{m}_{F,g} = \dot{m}''_{F,f} A_f \qquad \text{[Flame-area method]} \qquad (5)$$

where the subscript f stands for flame and F for fuel, $\dot{m}''_{F,f}$ denotes the mass flux of fuel gas on the flame surface, and A_f stands for the area of the flame sheet. The accurate use of this flame-area method has several requirements, (1) the reaction rate must be fast so that the flame is thin (sheet) and its surface A_f can be measured, and (2) $\dot{m}''_{F,f}$ should be nearly constant for a given fuel and flame configuration, though it may increase with the local airflow strain rate of the diffusion flame (or the oxygen supply to the flame sheet, considering the near-stoichiometric nature of the diffusion flame). Nevertheless, if the primary driving force to bring the oxygen and fuel to flame is diffusion (e.g., in microgravity), the value of $\dot{m}''_{F,f}$ could be stable and nearly constant that can be calibrated.

Once the fuel burning rate ($\dot{m}_F$) is quantified, the flame HRR can be given by:

$$HRR = \eta \dot{m}_F \Delta H_c \tag{6}$$

where η is the combustion efficiency and ΔH_c is the fuel's heat of combustion. In summary, the above three methods for measuring the burning rate of condensed fuels (Eqs. 3-5) do not require measuring the weight loss of the condensed fuel that may be used in the microgravity spacecraft environment. Instead, they need the values of A_f, v_f and $\dot{R}_F$, which can be measured based on the camera recording of fuel and flame, as well as the imaging processes.

Besides, the flame HRR can also be indirectly measured by oxygen calorimetry as

$$HRR = \Delta \dot{m}_{O2} \Delta H_{ox} \tag{7}$$

where $\Delta \dot{m}_{O2}$ denotes the change in the oxygen mass flow rate before and after the burning, and ΔH_{ox} = 13.1 kJ/g is the heat of oxidation for most hydrocarbon fuels with a relative uncertainty of 10%.

2.2. Experimental design

The experiments to verify the applicability of the above outlined three balance-free methods to measure MLR (Eqs. 3-5) were first conducted in a normal-gravity room environment (25 ℃, 1 atm). Of a large number of microgravity PMMA-flame data in the literature [14–21], the PMMA rods [14] with diameters of 8-15 mm were defined as the main target fuels. Besides, a solid candle, liquids including propanol, hexane, and kerosene, and gases including methane and propane were all used for comprehensive verification of the concept. To control the flames of different fuels, different burners were used (Figs. 2a-c). Specifically, glass tubes with varying diameters were employed for liquid fuels, and typical tubular gas burners were used to produce diffusion gas flames. The tested flame HRR ranges from 34 W (candle flame) to 490 W (thick-PMMA flame). The key parameters of fuel, burner and flame are listed in Table 1, and all flames in this work were laminar.

A propane torch was used to ignite all fuels from the top. A digital camera with a resolution of 1920×1080 pixels and a shutter speed of 50 fps was used to monitor both the fuel and flame. For solid fuels (Fig. 2a), they could take from several seconds (for candle) to several minutes (for thick PMMA rod) to attain a steady-state flame. For the liquid fuels in test tubes (Fig. 2b), the flames gradually

became smaller and weaker as the liquid level descended, so the liquid flames were monitored persistently from ignition to extinction. For gas fuels (Fig. 2c), to ensure the flame was stable after the ignition or the change of fuel flowrate, the flame was burnt for 3 mins before the start of measurement.

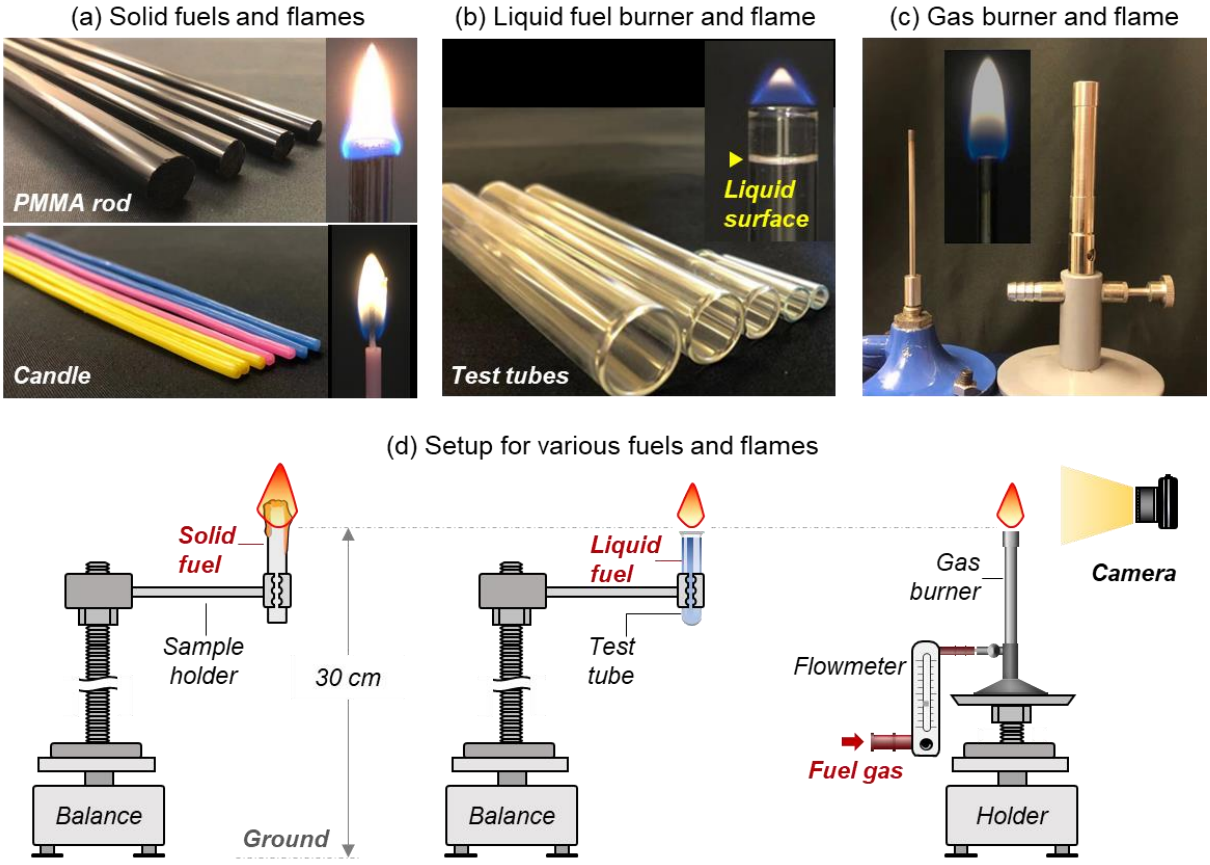

Fig. 2. (a) PMMA rods and candle, (b) liquid-fuel tubes and flame, (c) gas burners and flame, and (d) illustration of experimental setups for different fuels.

For the calibration of the mass-loss rate in Earth gravity, all solid and liquid fuels and burners were fixed by holders to a position where their tops are 30 cm from the ground. A precision mass balance (load cell) that works from 0-1000 g with an accuracy of 1 mg was mounted below the holders to measure the actual MLR for solid and liquid fuels ($\dot{m}$ in Eq. 1). For calibrating the burning rate of gaseous fuels, a flowmeter was used to control the fuel volume flow rate to the gas burner ($\dot{V}_{F,g}$ in Eq. 2). All flames were measured at least three times to reduce the random error and calculate the uncertainty. To further quantify the accuracy of each method, the root-mean-square error (ε) of $\dot{m}_F$ in Eq. (3-5) was calculated by comparing with $\dot{m}$ from balance or flowmeter as

$$\varepsilon = \sqrt{\frac{1}{n}\sum_{i=1}^{n}(\dot{m}_F - \dot{m})^2} \tag{8}$$

where n is the number of sampling data.

Table 1. The tested flame cases using different fuels at different sizes.

Fuel type	Fuel name	Fuel density [g/cm^3]	Fuel length[#] [mm]	Fuel diameter[#] [mm]	Flame height [mm]	Flame HRR* [W]
Solid	PMMA	1.21	200	8, 10, 12, 15	8.0 – 9.8	299 – 490
	Candle	0.90	100	3	16.0	34.0
Liquid	Propanol	0.80	30 – 100	3, 5.3, 8.0, 11, 16	1.2 – 37.8	34.0 – 161
	Hexane	0.66	30 – 100	3, 5.3, 8.0, 11, 13	7.2 – 90.7	48.3 – 184
	Kerosene	0.81	30 – 100	3, 5.3, 8.0, 11, 13	5.1 – 36.2	32.3 – 120
Gas	Methane	0.65×10^{-3}	100	3, 12.8	5.0 – 20.0	13.4 – 51.2
	Propane	1.81×10^{-3}	100	3	10.0 – 65.0	7.0 – 76.0

[#] Tube length and diameter are used for liquid fuels, and nozzle length and diameter are used for gaseous fuels.

[*] The maximum HRR is used for solid and liquid fuels.

2.3. Imaging analysis

Although the camera can only depict flame on a 2-D plane, the flame area A_f can be reconstructed based on a 3-D flame sheet with an in-house MATLAB imaging-process code. An image of a flame of a 12-mm diameter PMMA rod at 12-s after ignition is shown in Fig. 3a as an example. First, the 2-D flame contour was extracted, and a 2-D Cartesian coordinate (x, y) was utilized to show the geometry, seen in Fig. 3b.

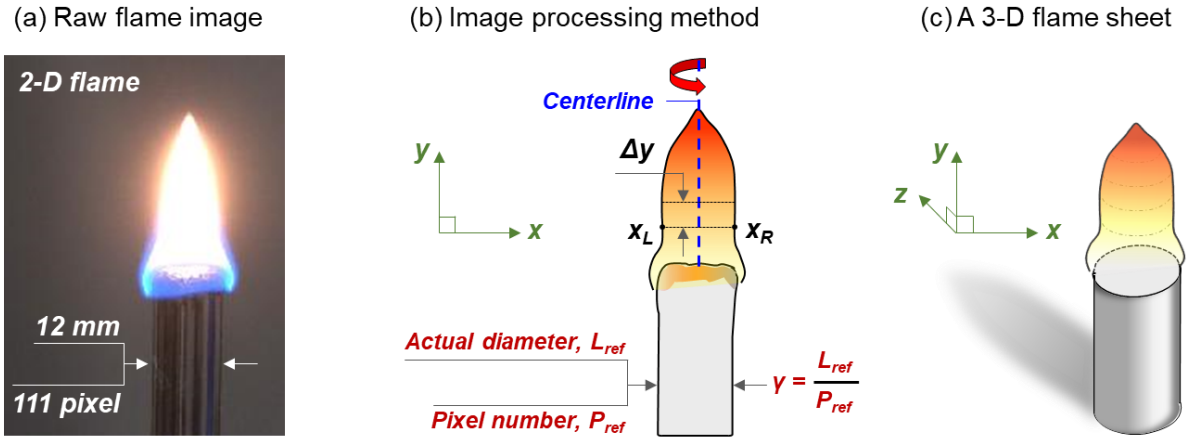

Fig. 3. (a) Image of a 12-mm PMMA flame, (b) rotation of a 2-D flame counter, and (3) a 3-D flame sheet.

By rotating the 2-D flame around its centerline into 3-D (Fig. 3c), the total flame-sheet area (A_f) can be given by an integration:

$$A_f = \sum \pi(x_R - x_L)\Delta y \gamma^2 \tag{9}$$

where x_L and x_R are the pixel positions of the leftmost and rightmost sides of the flame counter at different flame height; $\Delta y = 1$ is the pixel step for integration along the flame centerline (y-direction);

and γ is the length/pixel ratio in the image (for example, $\gamma = 0.11$ mm/pixel in Fig. 3a). Note that knowing the geometrical information is helpful for all these visual-based methods. Herein, the axial symmetry of flame shape, fuel, and leading edge simplifies the imaging analysis and improves the accuracy of estimation. If two or more cameras are used to take photos from different directions, the accuracy of the image-based measurement can be further improved.

3. Results in normal gravity

3.1. MLR estimation of a burning candle (base case)

The flame produced by a 3-mm candle was first analyzed to directly compare the $\dot{m}_F$ calculated with the three balance-free methods to the $\dot{m}$ measured by the load cell. A thin candle as the base case was selected because it can melt and produce a stable laminar flame without dripping. Besides, the candle flame has a wick (see Fig. 4), which keeps a distance between the flame and fuel top surface, so both the flame and the fuel-regression surface can be clearly captured by the camera.

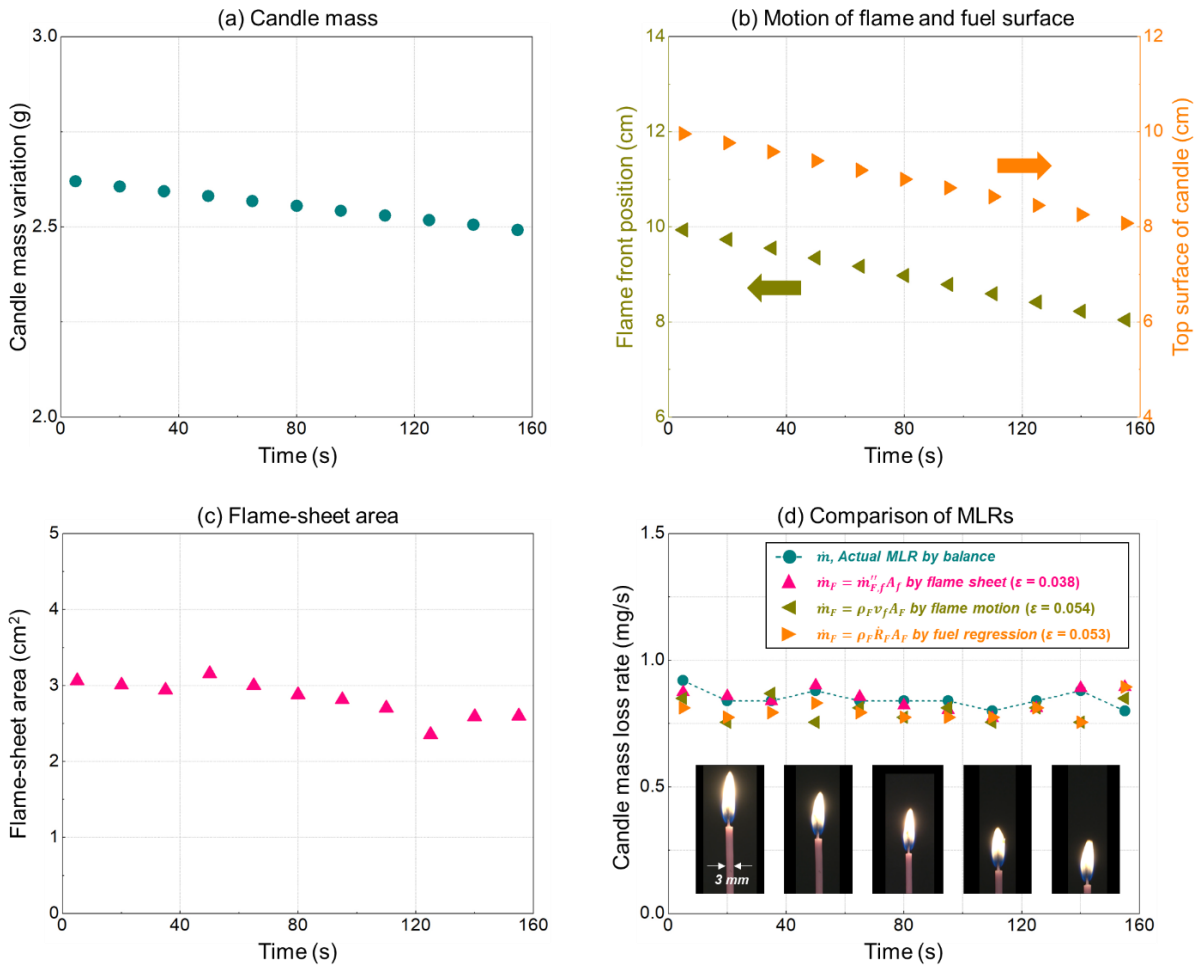

Fig. 4. (a) Mass variation of candle by balance, (b) positions of flame and fuel surface to the candle bottom, (c) variation of flame-sheet area, and (d) the measured and predicted candle mass-loss rate.

The burning rates ($\dot{m}_F$) predicted by the three balance-free methods for a candle are presented in Fig. 4 and compared with the $\dot{m}$ measured by balance. The small discrepancies ($\varepsilon < 0.06$) between the balance measurement and method predictions support the application potential for each method. In particular, the mass flux of candle vapor keeps $\dot{m}''_{F,f} = 0.29$ mg/cm^2-s, given by the ratio of candle mass loss (Fig. 4a) to candle flame area (Fig. 4c), leading to the smallest uncertainty ($\varepsilon = 0.038$) in the prediction from Eq. 5, which equals an HRR error of around 1.6 W. Comparatively, the measurements based on the flame motion and fuel regression have a larger fluctuation. Such a fluctuation increases if the sampling time decreases, because of a smaller change in the flame and fuel-surface position.

3.2. Flame-area-based MLR estimation for PMMA

The PMMA rods with parameters listed in Table 1 were then investigated. As reported by Huang et al. [19], the PMMA flame on Earth has a very low regression rate unless it experiences a large opposed flow. Therefore, both the flame and the regression surface over the PMMA rod can be entirely viewed with the camera, similar to the candle.

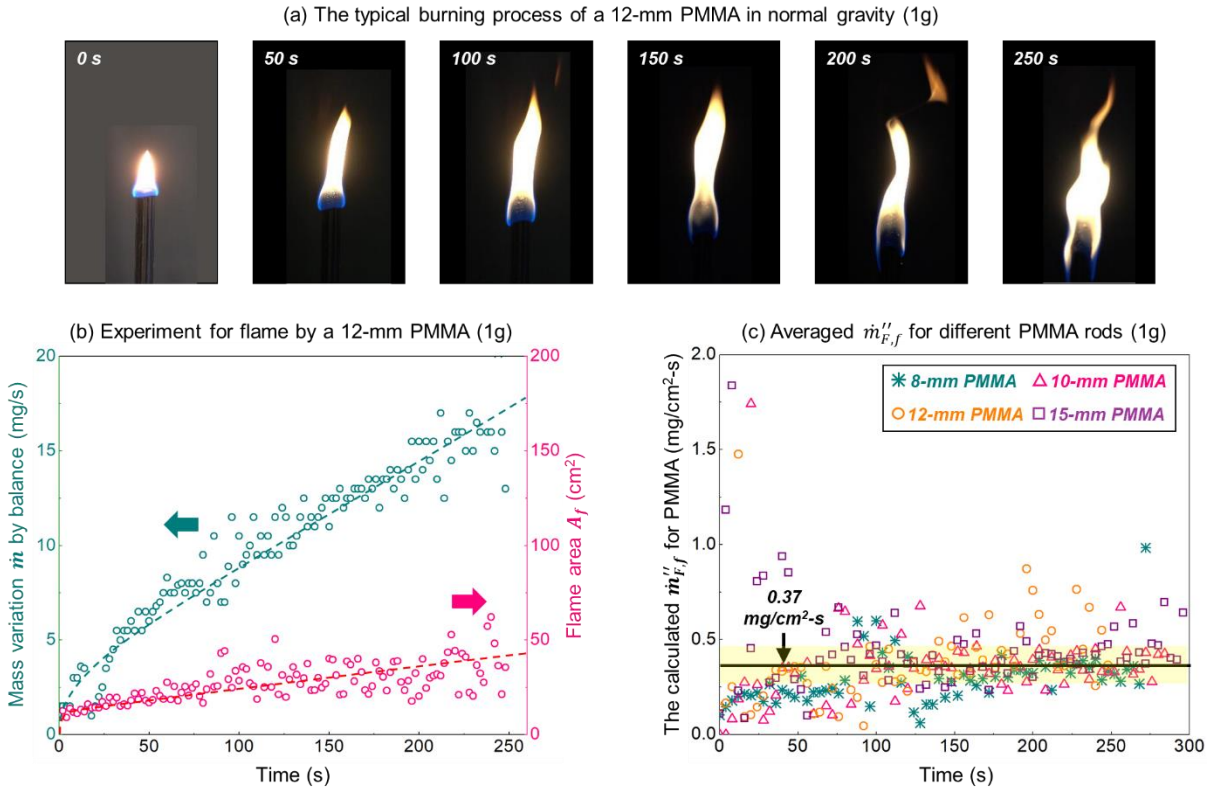

Fig. 5. The dependence of $\dot{m}''_{F,f}$ on fuel diameter in normal gravity, including (a) typical burning of a 12-mm PMMA, (b) measured MLR and flame area, and (c) $\dot{m}''_{F,f}$ obtained for all PMMA rods.

A sequence of the flame snapshots of a flame spreading over a 12-mm PMMA rod is presented in Fig. 5a. As can be seen, the flame cannot reach a stable state before the PMMA starts to melt, and consequently, the flame keeps growing with time, combined with fluctuations propagating in the

streamwise direction. Hence, the flame area A_f captured shows a positive dependence on time, despite of some data fluctuation, as shown in Fig. 5b. This trend is also observed in the PMMA mass variation $\dot{m}$ recorded by the balance, also shown in Fig. 5b. However, the fluctuations are not caused only by buoyancy puffing but also by the bursting and bubbling on the plastic surface, which also exist in microgravity experiments [7].

The calculated $\dot{m}''_{F,f}$ is shown in Fig. 5c, which is given by the ratio of $\dot{m}/A_f$. Besides the $\dot{m}''_{F,f}$ for a 12-mm PMMA, those for other PMMA rods are also presented. For all cases, $\dot{m}''_{F,f}$ will only fluctuate within a specific range of mass flux from 0.1-1 mg/cm^2-s as time evolves. Specifically, a majority of the data tend to converge to 0.37 ± 0.08 mg/cm^2-s, especially in the flame stage after initial ignition. This result supports that $\dot{m}''_{F,f}$ could be taken as constant during the burning of a given condensed fuel, irrespective of the fuel size. Thus, with this data-driven approach, $\dot{m}''_{F,f} = 0.37$ mg/cm^2-s was used to predict the MLR of burning PMMA in normal gravity.

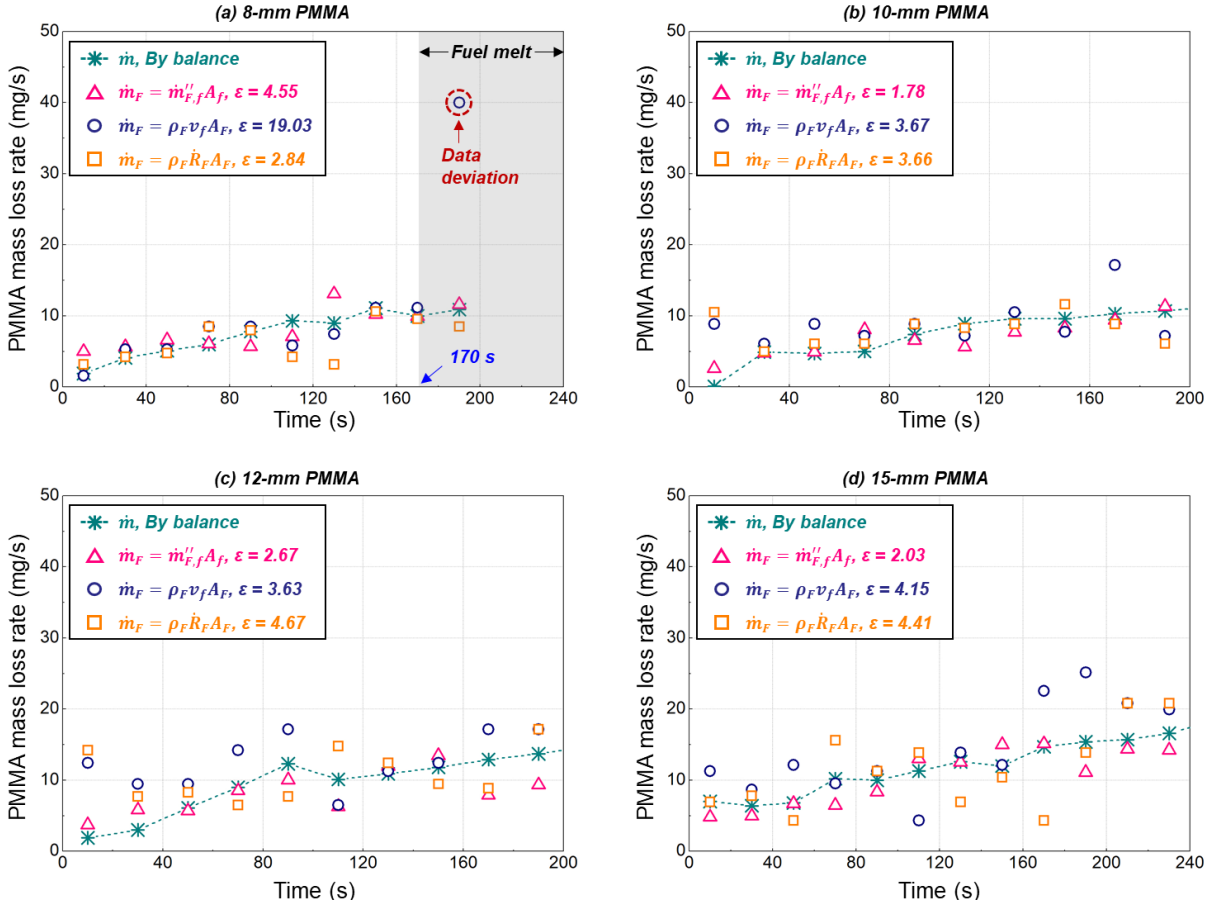

Fig. 6. A comparison of the measured and predicted MLRs for different PMMA cases.

Fig. 6 compares the $\dot{m}$ measured by the balance and the $\dot{m}_F$ predicted by Eqs. (3-5) for different PMMA rods. The deviation (ε) for each prediction is also given, where the sampling number is defined by a time step of 20 s during experiments. A first glance at Fig. 6 allows again confirming the excellent prediction of all the methods. Before the fuel melts, the flame-area method (Eq. 5) is again found to be

the most accurate among all methods, as it has the smallest ε. However, to comprehensively evaluate the pros and cons of Eq. (5), its performances in liquid and gas fuels are also discussed.

3.3. Flame-area-based MLR estimation for liquids and gases

As mentioned before, specific burners were used to produce controllable liquid and gas flames. Fig. 7a takes a propanol flame as an example, produced in an 8-mm test tube. It can be found that the liquid level inside the tube gradually decreases as the flame develops. In this condition, it is easy to imagine that the heat flux from the flame into fuel also decreases, leading to a reduction of fuel evaporation and flame area. By contrast, the gas burner can support a very stable flame, e.g., the propane-air flame in Fig. 7b. It should be noted that since there is no fuel regression for gas flames, the flame-area method (Eq. 5) is the only one that works for flames in all gas, liquid, and solid fuels.

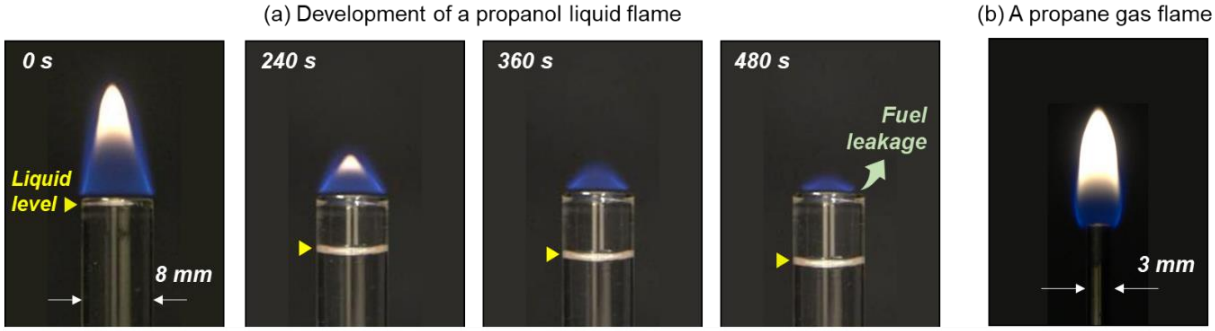

Fig. 7. (a) A propanol flame in an 8-mm test tube, and (b) a propane flame by a 3-mm gas burner.

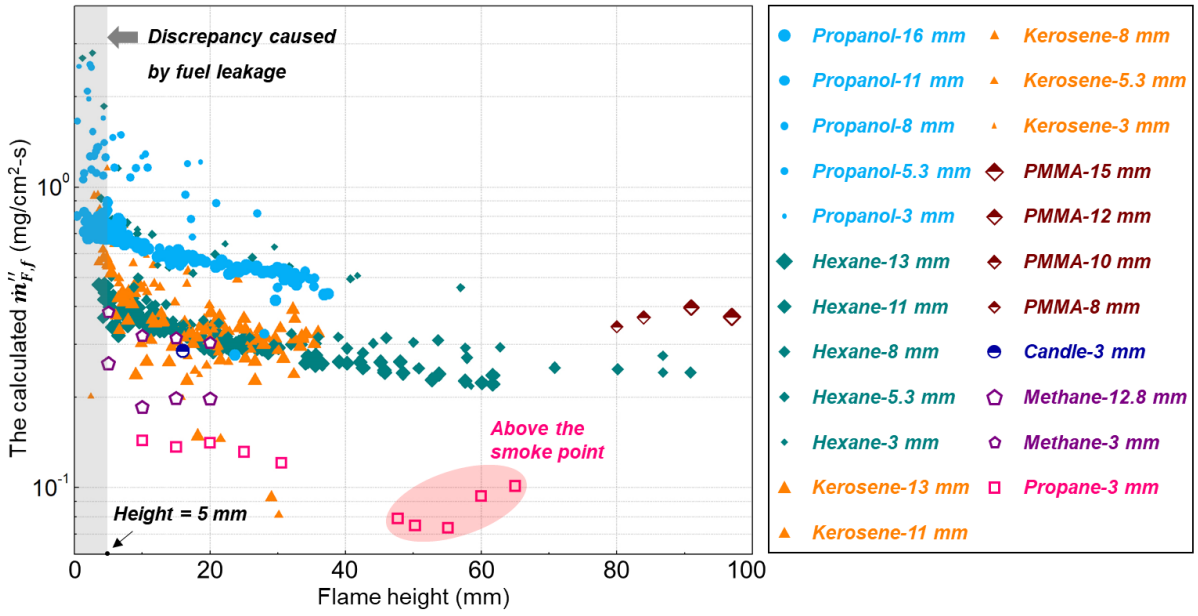

Fig. 8. Dependence of $\dot{m}''_{F,f}$ on flame height, where the size of the symbol reflects the size of the burner.

Here, it is still required to check if $\dot{m}''_{F,f}$ can be constant for a given fuel. Fig. 8 summarizes the calculated $\dot{m}''_{F,f}$ vs. flame height for all the tested gases, liquids, and solids, where the relative size of

the symbol represents the size of the fuel or burner used. For liquid fuels, all their $\dot{m}''_{F,f}$ manifest a converging tendency to a specific stable value that depends on the fuel type. Moreover, a stable $\dot{m}''_{F,f}$ can only exist when the liquid flame remains a height larger than 5 mm. For lower flames, their $\dot{m}''_{F,f}$ are sharply increased. This is because when the liquid flame becomes weak, the flame sheet cannot completely cover the opening of the tube, see Fig. 7a at 480 s. In this case, not all the evaporated fuel is consumed at the flame. Some may leak from the flame edge but are still measured and used to calculate $\dot{m}''_{F,f}$.

As for gas fuels, it is found that their $\dot{m}''_{F,f}$ depends not only on fuel type but also on burner diameter. Furthermore, experiments on propane reveal that the $\dot{m}''_{F,f}$ in gas flame can be further influenced by smoke generation. However, the flowmeter can still work in microgravity, so using Eq. (5) to describe a gas flame, although unnecessary, is used here for comparison purposes only.

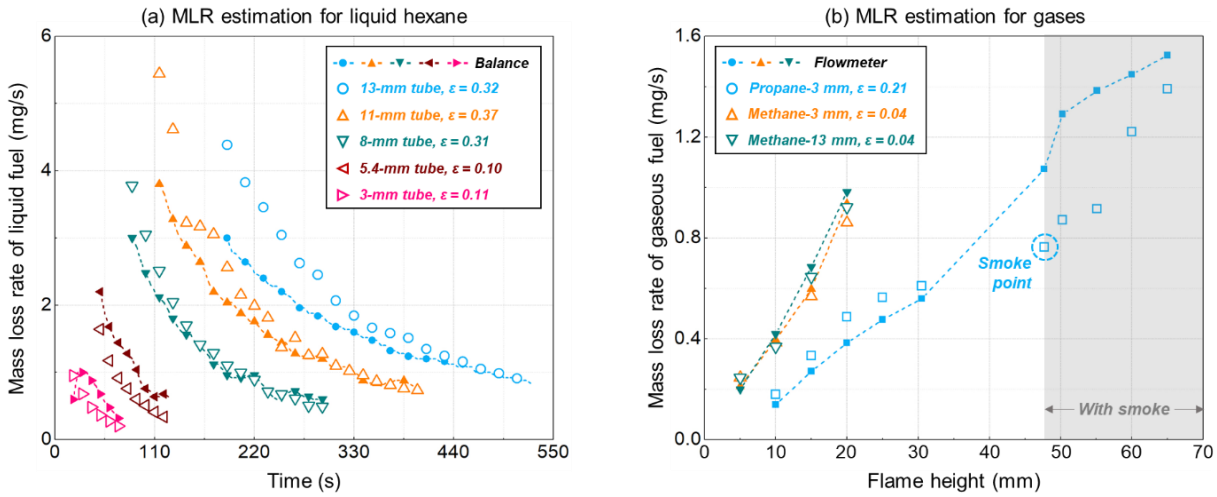

Fig. 9. Comparison of the MLR estimations by the flame-area method (Eq. 5) with (a) balance-based measurements for hexane in different test tubes, and (b) flowmeter-based measurements for propane and methane in different gas burners.

Fig. 9a takes hexane as an example of liquid fuels and compares the $\dot{m}_F$ by Eq. (5) with the $\dot{m}$ by the balance. The $\dot{m}''_{F,f}$ for hexane was calculated as 0.35 mg/cm^2-s, based on the results in Fig. 8 when the flame is larger than 5 mm. For clarity, the starting time of each curve is staggered. As can be seen, there is a wide range of conditions where the prediction by the flame-area method (Eq. 5) is in good agreement with the actual MLR. Moreover, in all cases, the maximum deviation (ε) for Eq. (5) is 0.32 mg/s, corresponding to an HRR error of around 15 W. As for the gas fuels, an accurate prediction can still be achieved below the smoke point.

3.4. Pros and cons for each method

According to all the above calibration experiments, the potential pros and cons for each method are summarized and listed in Table 2. Specifically, the mechanism behind the advantage of Eq. (5)

compared with the other two methods is given. In fact, the excellent predicting of the flame-area method (Eq. 5) can be mainly attributed to its response to the burning behavior of solid fuels. Reexamining Fig. 6a, the last data point given by the flame-spread method (Eq. 4) deviates significantly from the balance measurement. This is due to the dripping of molten PMMA, which will cause a sudden increase in the flame spread rate. Although the dripping of PMMA cannot occur in microgravity, there may be other burning behavior that could lead to the same disturbance, such as PMMA bursting [7]. However, these unstable burning behaviors of plastic fuels are local and will not excessively affect the whole flame area, so the use of the flame-area method (Eq. 5) is not affected much.

Table 2. Pros and cons for different MLR estimation methods in microgravity.

Methods (in μg)	Balance (Eq. 1)	Flowmeter (Eq. 2)	Fuel regression (Eq. 3)	Flame spread (Eq. 4)	Flame area (Eq. 5)
Formula	$dG/(gdt)$	$\rho_{Fg}\dot{V}_{F,g}$	$\rho_F \dot{R}_F A_F$	$\rho_F v_f A_F$	$\dot{m}''_{F,f} A_f$
Solid fuel	×	×	√	√	√
Liquid fuel	×	×	√ (If fuel level is visible)	×	√
Gas fuel	×	√	×	×	√
Accuracy	-	High	Not high (affected by time delay and bubbling)	Not high (affected by unstable burning)	High (if $\dot{m}''_{F,f}$ is known)
Dependence on background light	-	-	Very high	High	Low
Sensitivity to camera resolution	-	-	Very high	High	Low
Response	-	Fast	Very slow	Slow	Fast

On the other hand, the use of Eq. (5) is found to be less reliant on background light. However, predicting MLR by tracking the flame leading edge and the fuel regression requires sufficient light to identify changes in the flame base and fuel. Moreover, the measurement of A_f can be achieved readily, while the measurements of $\dot{R}_F$ and v_f should take time to allow for an obvious structural change in the fuel and flame. This means Eq. (5) has a faster response than the other methods. In sum, the flame-area method appears to be the top performer to assess the burning MLR in microgravity.

4. Demonstration of PMMA flame in microgravity

In our previous works [14,19], the microgravity tests on PMMA flame have been conducted in the International Space Station (ISS) as a part of the Burning and Suppression of Solids-II (BASS-II) project [16–18], which is intended to understand the mechanism that governs the flame spread over the surface of solid combustible materials. The tests were carried out with rods of black PMMA with diameters of 6.4 mm, 9.5 mm, and 12.7 mm and a length of 57 mm. Due to the absence of gravity, opposed flows

with velocities from 4 – 76 mm/s and oxygen concentrations between 17-21% were used to support the flame spread. Two oxygen sensors were implemented in the working volume for O_2 measurement [30].

Figs. 10a-b shows the developments of PMMA flames in space as an example, which also shows the unique flame structure in microgravity with an open tip. The data recorded previously include flame videos, flame spread rates, and the flame HRRs estimated using oxygen calorimetry. These data can be used here to estimate the MLR and HRR based on the flame spread and fuel regression and to check whether $\dot{m}''_{F,f}$ remains constant for the use of the flame-area method. Fig. 10c replots the flame HRRs for BASS-II PMMA rods in microgravity based on the oxygen calorimetry [30], which in general increases with the oxygen concentration from 20 W at 17% O_2 to 50 W at about 21% O_2.

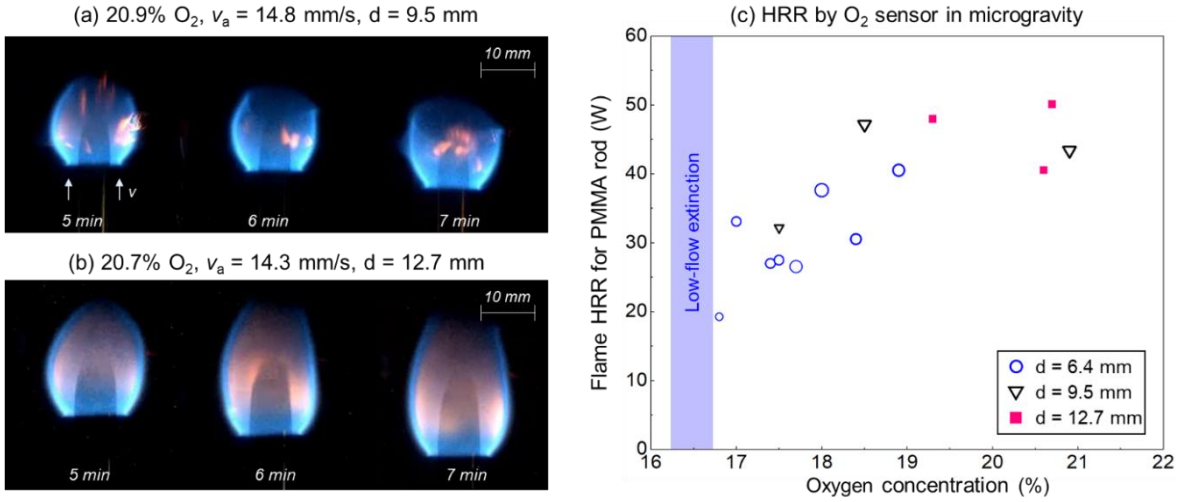

Fig. 10. Flame spread in microgravity for (a) 9.5-mm and (b) 12.7-mm PMMA rods, and (c) the summary of the flame HRR vs. oxygen concentration, opposed flow velocity and rod diameter [30] in microgravity, where the size of the symbol represents the relative amplitude of opposed flow velocity.

4.1. Estimation based on the fuel-regression rate

The fuel-regression method (Eq. 3) was first used to predict the MLR for PMMA rods in the microgravity experiments. The transient MLR evolution of a 6.4-mm PMMA is plotted in Fig. 11a versus time (see data of 9.5-mm and 12.7-mm rods in Supplemental Materials). The prediction from the flame-area method (Eq. 5) was also given as a comparison, where the value of $\dot{m}''_{F,f}$ used will be discussed later in Fig. 13. In general, both methods produce a similar overall trend of MLR, but the prediction from the fuel regression has much greater fluctuation. Such a fluctuation will further increase if the time interval between measuring points is reduced.

There are two reasons that contribute to the fluctuations, (1) there is a strong bubbling and bursting process on the burning surface of PMMA that can change the local shape of the fuel; and (2) with a weak background light and limited resolution of the camera, it is difficult to accurately determine the exact fuel surface. Fig. 11b summarizes all the HRR calculated from the fuel-regression method and compared with the oxygen calorimetry methods [30] for all microgravity data with 6.4-mm PMMA rod.

As expected, a large variation is found for the fuel-regression method, especially for cases with lower image quality. Nevertheless, if there is enough background light and a high image resolution in spacecraft, the accuracy of the fuel-regression method can be improved.

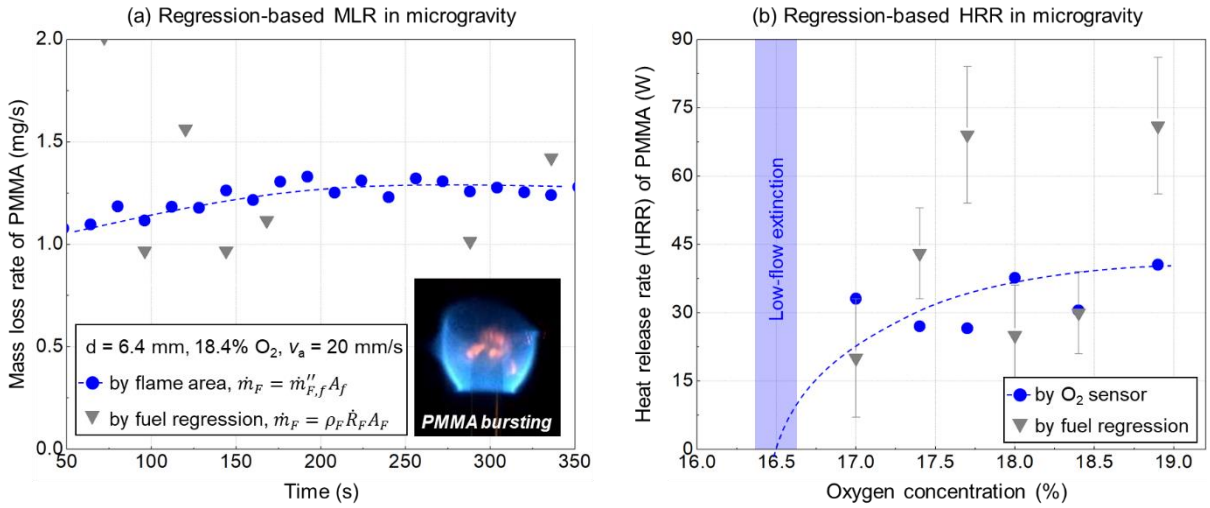

Fig. 11. (a) Evolution of the microgravity MLRs based on fuel regression and flame-sheet area, and (b) estimated HRR from fuel regression and oxygen calorimetry, with the error bar calculated by the MLR fluctuation; the PMMA rod diameter is 6.4 mm, and opposed flow is about 20 mm/s.

4.2. Estimation based on the flame-spread rate

To evaluate the feasibility of the flame-spread method (Eq. 4), Fig. 12a replots the opposed flame spread rate for a 6.4-mm PMMA rod in both normal-gravity and microgravity environments [14], where the flame spread rate increases with increasing oxygen concentration. Because of extending the extinction limit to a lower oxygen concentration, the flame spread rate in microgravity is higher than that in normal gravity (discussed more in [14]). Then, based on the flame spread rate and Eqs. (4) and (6), the flame HRR in microgravity can be estimated.

Fig. 12b compares the microgravity HRR from the flame-spread method and the oxygen-calorimetry method. For comparison, the HRRs of PMMA-rod flames based on the mass balance in normal gravity are also given, which are much larger than the HRR from the oxygen calorimetry in microgravity. This result agrees with experimental observation, where the PMMA flames in normal gravity are much stronger and brighter than those in microgravity.

Fig. 12b also shows that the flame-spread method (Eq. 4) significantly overestimates the HRR in microgravity, which is 2-3 times greater than that from the oxygen-calorimetry method. This is because, during the BASS-II microgravity tests, the burning time under a given flow condition was relatively short (only 1~3 min), so the burning rate had not reached the steady-state for the new flow condition (usually 5-10 min is needed based on experiments in normal gravity). In contrast, when the airflow velocity or the oxygen concentration changes, the flame spread rate can reach a new steady state within a few seconds. As such, Eq. (4) becomes inaccurate because the transient flame-spread rate no longer

reflects the real-time burning condition. Similar results for 9.5-mm and 12.7-mm rods can be found in Supplemental Materials. Thus, the flame-spread method may not give an accurate HRR estimation in microgravity, as the most of microgravity flame-spread experiments have a short burning duration.

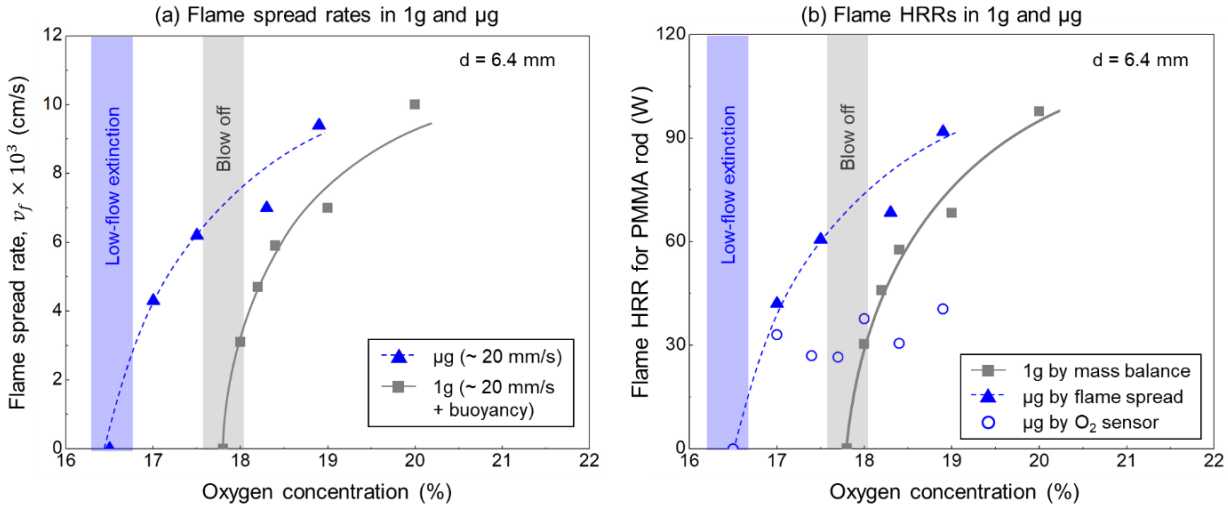

Fig. 12. (a) Opposed flame spread in microgravity (μg) and normal gravity (1g) vs. oxygen concentration [14], and (b) the HRRs estimated from the flame spread rate and the oxygen calorimetry [30], where PMMA rod diameter is 6.4 mm, and opposed flow is about 20 mm/s.

4.3. Estimation based on the flame-sheet area

The validity of estimating MLR and HRR by the flame-sheet area depends on the assumption of constant mass flux of fuel gas at the flame surface ($\dot{m}''_{F,f}$). Thus, it is important to calculate the $\dot{m}''_{F,f}$ in microgravity. Based on the HRR from the oxygen calorimetry and Eqs. (5-7), the $\dot{m}''_{F,f}$ in microgravity can be given by

$$\dot{m}''_{F,f} = \frac{HRR}{\eta \Delta H_c A_f} = \frac{\Delta \dot{m}_{O2} \Delta H_{ox}}{\eta \Delta H_c A_f} \tag{10}$$

where the combustion efficiency is assumed as η = 1, A_f comes from video processing, and $\Delta H_c = 25.1$ kJ/g is the common heat of combustion for black PMMA [33].

Fig. 13 shows the calculated $\dot{m}''_{F,f}$ for the microgravity flame of PMMA rods in the BASS-II experiments, where the small (opposed) airflow velocity is 10-20 mm/s. In addition, the range of $\dot{m}''_{F,f}(1\text{g}) = 0.37 \pm 0.08$ (mg/cm^2-s) obtained from the normal-gravity experiments (Fig. 5c) was also presented as a comparison. In general, the fuel mass flux at the flame sheet is smaller due to a smaller strain rate, and it is almost constant under a small low-airflow microgravity environment, i.e., $\dot{m}''_{F,f}(\mu\text{g}) = 0.15 \pm 0.03$ mg/cm^2-s. Thus, it can be concluded that the assumption of constant fuel mass flux at the flame surface is reasonable for microgravity PMMA flame under a small airflow. On the other hand, the value of $\dot{m}''_{F,f}$ in microgravity is much smaller than that in normal gravity. It is probably

because in normal gravity, the strong and complex buoyancy flow can stretch the flame sheet more to consume more fuel gas per unit area.

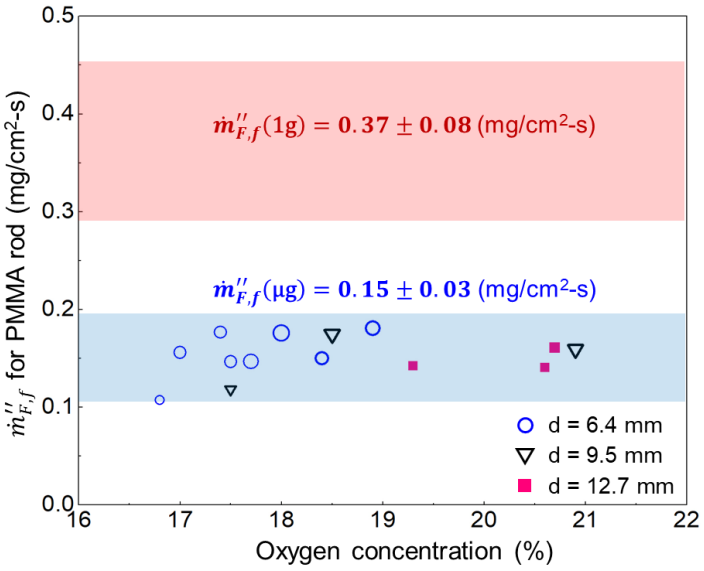

Fig. 13. The calculated fuel mass flux at the flame surface ($\dot{m}''_{F,f}$) for the PMMA flame in both the microgravity BASS-II experiments and the ground-based experiments of this work, where the size of the symbol represents the relative magnitude of opposed flow velocity from 10 - 20 mm/s.

In short, these results provide a basis for using the flame-area method (Eq. 5) to estimate the fuel MLR and flame HRR in microgravity, although further verifications are needed with more microgravity experiments on different fuels and complex flames. In addition, the numerical fire modelling can be conducted to quantify the local fuel-gas mass flux on the flame sheet and further evaluate the accuracy and boundary of this flame-sheet approach. Eventually, a more accurate evaluation method of flame HRR can help design future spacecraft combustion experiments and simulate possible spacecraft fires.

5. Conclusions

This paper is motivated by estimating the burning MLR of condensed combustible materials in microgravity, where the fuel weight loss cannot be used in assessing the flame HRR. Three potential alternate methods are proposed, i.e., (1) by measuring the spread rate of the flame leading edge, (2) by measuring the regression rate of condensed fuel, and (3) by measuring the area of the flame sheet.

The feasibility of each method has been first examined by calibration experiments in normal gravity with typical gas, liquid, and solid fuels. Results show that the methods based on flame spread and fuel regression can both accurately predict the MLR of condensed fuels, but the prerequisites include sufficient background light, no fuel melting and dripping, and below the smoke point. In contrast, the flame-area method is convenient to assess the burning MLR with few influencing factors, and the required parameter, i.e., the fuel mass flux at the flame sheet ($\dot{m}''_{F,f}$) could be constant for a given fuel configuration and environment.

The microgravity flames on PMMA rods (from the BASS-II project conducted in the International Space Station) were then used to further verify the methods proposed. Results show that the MLR obtained optically by tracking fuel regression has a large variation and is very sensitive to camera setting and resolution, as well as the background light. The MLR obtained optically by tracking the flame leading edge requires the burning rate to reach the steady state, so the results are often less accurate and with a substantial delay. Comparatively, the flame-area method performs best in accessing the MLR of PMMA rods and estimating the HRR in microgravity, because the required parameter $\dot{m}''_{F,f} \approx 0.15$ mg/cm^2-s is constant and more stable than that on Earth. Note that all image-based methods by default are sensitive to camera and environmental conditions, and an alternative method could be using the oxygen calorimetry if a wind tunnel is used. This work helps understand the fire dynamics in microgravity by exploring different ways to measure flame HRR in spacecraft and provides a path for the performance-based spacecraft fire safety design.

Acknowledgments

C.X. is funded by the National Natural Science Foundation of China (NSFC) Grant No. 52006185; X.H. is funded by HK PolyU Emerging Frontier Area (EFA) Scheme of RISUD (P0013879), and CFP is supported by NASA Grants NNX10AE01G and NNX13AL10A.

CRediT author statement

Caiyi Xiong: Investigation, Writing - Original Draft, Formal analysis. **Haoran Fan:** Investigation, Resources. **Xinyan Huang:** Methodology, Conceptualization, Formal analysis, Supervision; Writing-Review & Editing. **Carlos Fernandez-Pello:** Methodology, Writing-Review & Editing.

Conflicts of interest

The authors declare that they do not have any conflicts of interest.

References

[1] Williams FA. Combustion Theory. 2nd ed. CRC Press; 1985.

[2] Jiang X, Luo KH. Combustion-induced buoyancy effects of an axisymmetric reactive plume. Proceedings of the Combustion Institute 2000;28:1989–95. https://doi.org/10.1016/S0082-0784(00)80605-0.

[3] Ross HD. Microgravity combustion : fire in free fall. Academic Press; 2001.

[4] Nayagam V, Dietrich DL, Ferkul P V., Hicks MC, Williams F a. Can cool flames support quasi-steady alkane droplet burning? Combustion and Flame 2012;159:3583–8. https://doi.org/10.1016/j.combustflame.2012.07.012.

[5] Urban DL, Ferkul P, Olson S, Ruff GA, Easton J, T'ien JS, et al. Flame spread: Effects of microgravity and scale. Combustion and Flame 2019;199:168–82. https://doi.org/10.1016/j.combustflame.2018.10.012.

[6] Dietrich DL, Nayagam V, Hicks MC, Ferkul P V, Dryer FL, Farouk T, et al. Droplet Combustion Experiments Aboard the International Space Station. Microgravity Science and Technology 2014;26:65–76. https://doi.org/10.1007/s12217-014-9372-2.

[7] Sun P, Wu C, Zhu F, Wang S, Huang X. Microgravity combustion of polyethylene droplet in drop tower. Combustion and Flame 2020;222:18–26. https://doi.org/10.1016/j.combustflame.2020.08.032.

[8] Fujita O. Solid combustion research in microgravity as a basis of fire safety in space. Proceedings of the Combustion Institute 2015;35:2487–502. https://doi.org/10.1016/j.proci.2014.08.010.

[9] Citerne J-MM, Dutilleul H, Kizawa K, Nagachi M, Fujita O, Kikuchi M, et al. Fire safety in space – Investigating flame spread interaction over wires. Acta Astronautica 2016;126:500–9. https://doi.org/10.1016/j.actaastro.2015.12.021.

[10] Dietrich DL, Haggard JB, Dryer FL, Nayagam V, Shaw BD, Williams F a. Droplet combustion experiments in spacelab. Symposium (International) on Combustion 1996;26:1201–7. https://doi.org/10.1016/S0082-0784(96)80336-5.

[11] Yang JC, Hamins A, Donnelly MK. Reduced gravity combustion of thermoplastic spheres. Combustion and Flame 2000;120:61–74. https://doi.org/10.1016/S0010-2180(99)00084-X.

[12] Huang X, Nakamura Y. A Review of Fundamental Combustion Phenomena in Wire Fires. Fire Technology 2020;56:315–60. https://doi.org/10.1007/s10694-019-00918-5.

[13] Vetturini A, Cui W, Liao YT, Olson S, Ferkul P. Flame Spread Over Ultra-thin Solids: Effect of Area Density and Concurrent-Opposed Spread Reversal Phenomenon. Fire Technology 2020;56:91–111. https://doi.org/10.1007/s10694-019-00878-w.

[14] Link S, Huang X, Fernandez-Pello C, Olson S, Ferkul P. The Effect of Gravity on Flame Spread over PMMA Cylinders. Scientific Reports 2018;8:120. https://doi.org/10.1038/s41598-017-18398-4.

[15] Wu C, Sun P, Wang X, Huang X, Wang S. Flame Extinction of Spherical PMMA in Microgravity: Effect of Fuel Diameter and Conduction. Microgravity Science and Technology 2020;32:1065–75. https://doi.org/10.1007/s12217-020-09829-5.

[16] Olson SL, Ferkul P V. Microgravity flammability boundary for PMMA rods in axial stagnation flow: Experimental results and energy balance analyses. Combustion and Flame 2017;180:217–29. https://doi.org/10.1016/j.combustflame.2017.03.001.

[17] Bhattacharjee S, Simsek A, Miller F, Olson S, Ferkul P. Radiative, thermal, and kinetic regimes of opposed-flow flame spread: A comparison between experiment and theory. Proceedings of the Combustion Institute 2017;36:2963–9. https://doi.org/10.1016/j.proci.2016.06.025.

[18] Olson SL, Ferkul P V, Bhattacharjee S, Miller FJ, Fernandez-Pello AC, T'ien JS. Burning and Suppression of Solids – II Fire Safety Investigation for the Microgravity Science Glovebox. 29th Annual Meeting of the American Society for Gravitational and Space Research (ASGSR) and the 5th International Symposium on Physical Sciences in Space (ISPS) 2013.

[19] Huang X, Link S, Rodriguez A, Thomsen M, Olson S, Ferkul P, et al. Transition from opposed flame spread to fuel regression and blow off: Effect of flow, atmosphere, and microgravity.

Proceedings of the Combustion Institute 2019;37:4117–26. https://doi.org/10.1016/j.proci.2018.06.022.

[20] Olson SL, Ferkul P V., Marcum JW. High-speed video analysis of flame oscillations along a PMMA rod after stagnation region blowoff. Proceedings of the Combustion Institute 2019;37:1555–62. https://doi.org/10.1016/j.proci.2018.05.080.

[21] Wu C, Huang X, Wang S, Zhu F, Yin Y. Opposed Flame Spread over Cylindrical PMMA Under Oxygen-Enriched Microgravity Environment. Fire Technology 2020;56:71–89. https://doi.org/10.1007/s10694-019-00896-8.

[22] Roper FG. The prediction of laminar jet diffusion flame sizes: Part I. Theoretical model. Combustion and Flame 1977;29:219–26. https://doi.org/10.1016/0010-2180(77)90112-2.

[23] Burke SP, Schumann TEWW. Diffusion Flames. Industrial & Engineering Chemistry 1928;20:998–1004. https://doi.org/10.1021/ie50226a005.

[24] Johnston MC, T'ien JS, James ST, T'ien JS. Gravimetric measurement of solid and liquid fuel burning rate near and at the low oxygen extinction limit. Fire Safety Journal 2017;91:140–6. https://doi.org/10.1016/j.firesaf.2017.03.027.

[25] Sunderland PB, Quintiere JG, Tabaka GA, Lian D, Chiu CW. Analysis and measurement of candle flame shapes. Proceedings of the Combustion Institute 2011;33:2489–96. https://doi.org/10.1016/j.proci.2010.06.095.

[26] Dehghani P, Quintiere JG. Theoretical analysis and predictions of burning in microgravity using a burning emulator. Combustion and Flame 2021;233:111572. https://doi.org/10.1016/j.combustflame.2021.111572.

[27] Quintiere JG. Fundamentals of fire phenomena. John Wiley; 2006. https://doi.org/10.1002/0470091150.

[28] Huggett C. Estimation of rate of heat release by means of oxygen consumption measurements. Fire and Materials 1980;4:61–5. https://doi.org/10.1002/fam.810040202.

[29] Jomaas G, Torero JL, Eigenbrod C, Niehaus J, Olson SL, Ferkul P V., et al. Fire safety in space-beyond flammability testing of small samples. Acta Astronautica 2015;109:208–16. https://doi.org/10.1016/j.actaastro.2014.11.025.

[30] Olson SL, Bhattacharjee S, Miller FJ. Experiment in the Microgravity Science Glovebox (MSG). International Conference on Environmental Systems 2015;45.

[31] Thomsen M, Fernandez-Pello C, Ruff GA, Urban DL. Buoyancy effects on concurrent flame spread over thick PMMA. Combustion and Flame 2019;199:279–91. https://doi.org/10.1016/j.combustflame.2018.10.016.

[32] Zhu N, Huang X, Fang J, Yang L, Hu L. Transitional flame-spread and fuel-regression behaviors under the change of concurrent wind. Fire Safety Journal 2021;120:103015. https://doi.org/10.1016/j.firesaf.2020.103015.

[33] Lyon RE, Hackett SM, Walters RN. Haet of Combustion of High-Temperature Polymers. Fire and Materials 2002;24:245–52.